Competitive Growth Texture of Pulse Laser Deposited VO_2 Nanostructures on Glass Substrate

B. D. Ngom [1-4], M. Chaker[4], I. G. Madiba[1-2], S. Khamlich[5], N. Manyala[5], O. Nemraoui[6], R. Madjoe[7], A. C. Beye[3], M. Maaza[1-2]

[1-]UNESCO-UNISA Africa Chair in Nanosciences-Nanotechnology, College of Graduate Studies, University of South Africa, Muckleneuk ridge, PO Box 392, Pretoria-South Africa,

[2-]Nanosciences African Network (NANOAFNET), iThemba LABS-National Research Foundation, 1 Old Faure road, Somerset West 7129, PO Box 722, Somerset West, Western Cape Province, South Africa.

[3-]Laboratoire de Photonique et de Nano-Fabrication, Faculté des sciences et Techniques Université Cheikh Anta Diop de Dakar (UCAD) B.P. 25114 Dakar-Fann Dakar, Senegal.

[4-]Institut National de la Recherche Scientifique Centre – Énergie Matériaux Télécommunications 1650, Boul. Lionel Boulet Varennes (Québec) J3X 1S2,

[5-]Department of Physics, SARCHI Chair in Carbon Technology and Materials, Institute of Applied Materials, University of Pretoria, Pretoria, South Africa.

[6-]Mechatronics, Cape Peninsula University of Technology, P O Box 1906, Bellville, 7530, South Africa.

[7-]Department of Physics, University of the Western Cape, Bellville, Cape Town, South Africa.

Abstract

We report on the crystal structure and morphology of VO_2 nanostructures synthesized by pulsed-laser deposition on soda lime glass. The VO_2 nanostructures exhibit sharp a-axis diffraction peaks, characteristic of the VO_2 monoclinic phase, which implies that highly a-axis textured VO_2 was formed. A detailed description of the growth mechanisms and the substrate/film interaction is given, and the characteristics of the electronic transition and hysteresis characteristics of the phase transition are described by the morphology and grain boundary structure. The sharpness of the transition and the hysteresis upon heating and cooling are found to be a strong function of crystal structure and microstructure (grain size, and shape).

Keywords

Crystal growth; Grains Growth; Texturation; Phase transition; Pulsed Laser deposition;

Corresponding author:

Dr. B. D. NGOM

UNESCO-UNISA Africa Chair in Nanosciences-Nanotechnology, College of Graduate Studies, University of South Africa, Muckleneuk ridge, PO Box 392, Pretoria-South Africa,
E-mail: bdngom@gmail.com

1. Introduction

Vanadium dioxide is a strongly correlated transition metal oxide with a first-order insulator-to-metal transition (IMT) at 67 ° C [1] and its potential applications ranging from femtosecond optical switching [2] to thermal-management coatings [3]. The IMT exhibits large changes in resistivity and near-IR transmission accompanied by a nearly simultaneous structural change from low-temperature monoclinic form with band-gap of about 0.7 eV [4] to a high temperature, tetragonal rutile phase. The phase transition is generally agreed to arise from the Mott mechanism [5, 6]. High-quality thin films are crucial for technologies that capitalize on the IMT. It is well known that film microstructure [7] film/substrate interface [8] and localized strain [9] of VO_2 can affect the hysteresis characteristics of the phase transition. VO_2 synthesis is also complicated by the narrow temperature-pressure window in phase space, due to multiple valence states of vanadium [10].

Due to the small compositional differences between numerous phases of vanadium oxides, VO_2 preparation requires a stringent controlled process that provides a desired oxygen stoichiometry and correct crystalline structure. In search of such a process, VO_2 films were produced by a number of methods, including dc and rf reactive magnetron sputtering [11–16] reactive ion-beam sputtering [17–21], reactive evaporation [22, 23], chemical vapor deposition (CVD) [24–26], pulsed laser deposition (PLD) [27–31], electrochemical (anodic) oxidation [32-33] and sol-gel process [34-36].

Within the requirement for an accurate optimization to obtain the correct VO_2 polycrystalline structure due to the multiple V electronic valences and its high affinity with oxygen, it is challenging to synthesize large thermochromic VO_2 based coatings, with such techniques. In an effort to produce large efficient and Ultraviolet radiation stable thermochromic coatings in addition to the cost effectiveness, pulsed laser deposition technique is also known for its dedication to the rational fast growth and its steochiometry transfer of advanced metal oxide particulate thin films and multi-dimensional arrays.

The resultant films structures varied depending on the crystallographic relationship between the growing VO_2 and the substrate, as well as on other factors, such as the growth temperature, some of the synthesis methods produced amorphous or quasiamorphous, others polycrystalline, and still others oriented epitaxial films. The best films [i.e., films with the highest ratio of resistivities in insulating and metallic phases and the smallest hysteresis width (ΔT_{IMT})] were prepared at 500–600 ° C on single-crystalline substrates having epitaxial relationship to the growing VO_2 [8-9]. Yet nonepitaxial, polycrystalline VO_2 films also exhibit the phase transition, although with a smaller *RR* and wider hysteresis. Surprisingly, the transition persists even in nearly amorphous films, such as in films obtained by anodic oxidation of vanadium. The transition in VO_2 is

apparently quite tolerant to the loss of long-range order. Of course, it ultimately depends on the intended application whether a film with a given transition is satisfactory or not, and often, when epitaxial growth is impossible or impractical, one has to compromise. Study of the literature shows that more often than not, initially obtained VO_x films were subsequently annealed in various atmospheres in air, in O_2, in Ar, in N, in order to obtain or to improve the VO_2 phase [18–22]. Once post annealing is employed, it appears logical to make a clean separation of metal deposition and subsequent oxide-forming annealing. Some films were produced in this way, by oxidation of vanadium metal precursor film and plates in air and in oxygen-argon mixtures [37–44].

This is the type of process we are using in this communication after a pre-depositing VO_x film via PLD using a Vanadium metallic target in pure background of oxygen. We found that upon proper optimization of the cooling substrate rate, good textured crystalline VO_2 films with a preferred orientation is synthesized. In the past, many films prepared by this method were found to have different layers such that from the upper surface, VO_2 was found to have a compositional gradient in *z* direction, with V in the bulk of the films, and lower oxides such as $VO_{0.5–1.0}$ near the lower interface [43]. A similar oxygen variation in *z* direction was found in anodic films [32-33]. It should be noted that precursors other than a metallic V were occasionally used. An interesting attempt to reduce or eliminate the *z* gradient by annealing a more complex $V_2O_5/V/V_2O_5$ precursor sandwich structure is described in reference [44]. In some publications the precursor is not a metal, but the highest V oxide, V_2O_5, and subsequent annealing is performed in vacuum rather than in O_2 in order to reduce it to VO_2 [45]. The latter requires performing oxidation in reduced pressure O_2. Slow oxidation of a vanadium precursor films in reduced air pressure was described previously in reference [41]. It appears that these films can be of a somewhat higher quality; possibly due to a replacement of air with oxygen.

In this paper we report on the PLD a-axis oriented VO_2 grown thin films influenced by substrate cooling rate in vacuum and in low pressure oxygen atmosphere which seems to affect the crystal structure, particle size and shape as well as the IMT characteristics of VO_2 films. It turns out that the growth of a-axis oriented VO_2 thin films on the glass substrate, have a direct bearing on the characteristics of the VO_2 thin films.

2. Experimental details

Films were deposited on soda lime glass substrate held at a temperature 600 ^{0}C in pure oxygen pressure of 15 mtorr at deposition time of 45 minutes. An excimer laser, wavelength of 248 nm, fluence of 1.7 J/cm^2, repetition rate of 10 Hz, and 30 ns pulse duration, was incident on V metal target. The substrates – target distance was kept

at 65 mm and the laser was focused to ablate the off-centre of the rotating target. After deposition the samples were cooled in vacuum by switching off the inlet oxygen gas at the same time pumping to vacuum at different cooling rate ranging from 5 ^{o}C/min to 25^{o}C/min. X-ray diffraction data of the same VO_2 specimens were collected on a laboratory D8 ADVANCE powder diffractometer in Bragg-Brentano geometry, operated at 40 kV and 40 mA using a Cu Kα radiation. The Goniometer set up including a Vantec-1 detector with N-filter and 4 degrees Soller slit providing narrow and symmetrical instrumental profiles (IP) over the required angular range. The XRD patterns of the samples were recorded in the range (2θ=12°–80°) using a step size of 0.02° and a counting time of 20s per step in each case without moving the sample. Qualitative phase analysis (search match) was done using the PANAlytical X'pert Highscore plus software employing the ICDD PDF database. The surface morphology was characterized via a Nova NanoSEM 230 scanning electron microscope (SEM) in secondary electron mode to investigate the surface morphology of the films after deposition and the UV-Vis-NIR spectroscopy data of the VO_2 samples were collected in the wavelength range of 350–1100 nm using a CECIL 2000 Spectrophotometer incorporated with Peltier thermoelectric heating and cooling stage.

3. Results and discussions

The XRD pattern characteristic of VO_2 thin films deposited on soda lime glass substrate and cooled down to room temperature at different rate of 5 ^{o}C/min to 25 ^{o}C/min under vacuum are presented in Fig 1. The pattern shows peaks due to thin layer at angles of 18.48, 27.97, 37.18, 39.98, and 57.048. Following the calculated pattern description of the monoclinic structure of VO_2 (JCPDS No: 43-1051), these peaks can be indexed as the reflections on (1 0 0), (0 1 1), (2 0 0), (0 2 0) and (0 2 2) planes respectively. The major diffraction peaks of the five samples are the same. The only difference lies in the relative intensity of the diffraction peaks. This is clearly indicated in Fig 2 where relative intensity of the (011) plane with respect to the (100) is plotted as a function of cooling temperature.

The preferential orientation along (1 0 0) of the VO_2 films deposited on soda lime glass substrate, is not clearly understood and have not been reported into the literature so far. G. Garry et al. [46] have controlled the crystallographic structure of VO_2, they reported an a-axis textured VO_2 thin films deposited on R-plane sapphire, where they observed all the (l 0 0) planes of VO_2. They suggested that the observation of all the peaks should be a stress developed into the interface between the substrate and the film. T.-W. Chiu et al. [47] have attempted to control the crystallographic orientation of VO_2 on glass. They reported VO_2 thin films deposited on a glass substrate and also on a 5 nm thick ZnO buffer layer deposited on a glass substrate both at 500^{o}C. On

their results, when VO_2 film was directly deposited on glass substrates, polycrystalline VO_2 films formed on the amorphous substrate surface and showed a preferential orientation along the (011) plane located at 27.87° in the XRD chart. When VO_2 thin films were deposited under 5.33 and 6.67 Pa O_2 pressure on 5 nm thick ZnO buffer, the polycrystalline random oriented VO_2 thin film formed, and only VO_2 (011) peaks located at 27.90 were observed. Their results reveal that b-axis oriented VO_2 film can be prepared under 1.33 Pa O_2 ambient using a c-axis oriented ZnO buffer but they were not able to grown VO_2 a-axis oriented on glass neither on the ZnO buffer layer. As they reported [47] the crystalline orientation of VO_2 thin films deposited on ZnO buffer was more sensitive to O_2 pressure during deposition. Even though the O_2 pressure was controlled within the range in which the pure VO_2 phase could be formed on c-cut sapphire and glass substrate, the crystalline orientation of VO_2 thin films was drastically changed because of the formation of an interface layer between VO_2 and ZnO. As a result in their experimental conditions no VO_2 a-axis oriented on glass were observed.

As reported in Fig 1, the extra peaks in some of the samples indicated by * at Bragg reflection at 2θ = 38.23°, could be associated with the presence of impurity phase. It should be noted that because of the multiple valence states of vanadium ions, can lead to several vanadium oxide phases such as Magneli phases (V_nO_{2n-1}) and Wadsley phases ($V_{2n}O_{5n-2}$), no other peak corresponding to any other vanadium oxide phases mentioned is present in the XRD spectra. H. Zhou et al. in their work [8] have identified a similar Bragg reflection at 2θ = 38.6° which they attributed as the (0006) reflection of V_2O_3. However, after a qualitative phase analysis (search match), done using the PANAlytical X'pert Highscore plus software employing the ICDD PDF database the only closest phase that could probably much the peak indicated by * is $Na_{1.80}V_2O_5$ (400) (JCPDS 0020-1167). Therefore we could speculate that this reflection at 2Θ= 38.23° also could indicate the presence of small amount of $Na_{1.80}V_2O_5$ phase in the thin films on soda-lime glass substrates, resulting from a diffusion of Na^+ into thin films from substrates due to high substrate temperature. S. Lu et al. [48], reported on the same impurity in their films of VO_2 with two small peaks at angle of 2θ = 12.1° and 2θ = 29.1° indicating the presence of small amount of $Na_xV_2O_5$ (with the value of 0.3<x>1.0) phase in the thin films on soda-lime-silica glass substrates. Wang Xue-Jin et al: [49], strongly concluded that sodium ions would diffuse from soda-lime substrate to film surface when sputter performed at high substrate temperature (580 °C in their experiment), which was in agreement with other authors who claimed that VO_2 film could not be deposited on soda-lime glass because of sodium contamination. Therefore we could suggest that, the peak at 2Θ= 38.23° indicate the presence of $Na_{1.80}V_2O_5$ phase in the thin films on soda-lime glass substrates, and is resulting from a diffusion of Na^+ into thin films from substrates during the thermal treatment of the substrate. But this conclusion does not account for the sample

cooled at 25 ^{o}C/min in which we can't see the peak marked by (*), this may be due the fact that in this sample the VO_2 thin films are highly crystalline and the intensities of the peaks (200) and (020) are too intense so that the (*) peak is absorbed and therefore can't be read on the XRD chart.

Fig.3A and 3B report on the evolution of the d-spacing along (100) and (011) planes respectively as function of the cooling rate. The crystallite grains sizes as function of the cooling rate along the same planes are depicted in Fig. 3C and 3D respectively. The reported values for the d-spacings agree with those of the monoclinic structure of VO_2 (JCPDS No: 43-1051). The influence of the cooling temperature is seen to have opposite effects when looking at the evolution of the crystalline size along the (100) and (011) planes as function of the cooling temperature (see Figs. 3C and 3D), while the influence on the d_{100} and d_{011} seems to have almost the same trend (see Figs. 3A and 3C).

Fig.4 reports the surface morphology of the deposited VO_2 on glass and cooled to room temperature with different cooling rate. It is observed that at low cooling rate, it is possible to synthesized different VO_2 nanostructures with different shape and sizes parallel to the substrate surface. However an increase in the cooling rate leads to a granular morphology type. The observed variation of the surface morphology of the VO_2 nanostructures with cooling rate as reported in Fig.4 may be due to the nucleation of the glass substrate which happens around 575^{o}C and followed by the process of crystallization of the VO_2 which follows the so called active fundamental structure forming phenomena well known in materials science and solid state physics (nucleation, crystal growth, grains growth) [50-54]. It is observed that the grains growth and the preferential texturation (crystal growth) are going to the opposite direction when increasing the cooling rate; this is supported by Figs. 1 and 3. Increasing the cooling rate lead to a preferential crystal growth along (100) plane while a longitudinal grains growth that lead to very well dispersed nanorods and naodisks-like parallel to the surface of the substrate is observed when decreasing the cooling rate.

The morphology and the growth direction of these nano-grains indicate that the surface crystallization starts off in a preferential direction. It is well known that the growth of thin films proceeds through consecutive stages characterised by specific processes of structure evolution: nucleation, island growth, coalescence of islands, formation of polycrystalline islands and channels, development of continuous structure and thickness growth. The evolution of the structure in polycrystalline thin films is a very complex phenomenon and exhibits different features in different stages of film growth.

By taking into account the structure evolution of real polycrystalline thin films [50–54] and that of the effects of the deposition parameter on the structure and on the appearance of peculiar structural features lead to the

conclusion that the comprehensive description of the formation of this peculiar structural features is possible by selecting the basic structure forming phenomena well known in materials science and solid state physics (nucleation, crystal growth, grain growth) [50–54]. These phenomena are composed of elementary atomic processes, and can give account for the global effects of the atomic processes on the structure evolution. It is important to note that the atomic processes are controlled directly not only by the temperature but also by the structural conditions characteristic of the actual growth stage.

The present results show that, as supported both by the SEM, XRD and the evolution of the crystalline growth along the (100) plane, the growth mechanism that can be considered here is the competitive texturation. The nucleation starting the growth of individual islands takes place on the substrate surface at the very first stage of the condensation (primary nucleation), and/or later on the bare substrate surface area developing upon liquid like coalescence (secondary nucleation). The primary nucleation starts the condensation and the film growth on the whole substrate surface simultaneously, while the secondary and the repeated nucleation initiates the starting of the growth locally in later stages of film formation. It is important to note that on amorphous substrates the nuclei are randomly oriented. The kinetics of nucleation is discussed in review articles in details [55–60]. Crystals growing from the nuclei are randomly oriented due to the random orientation of the nuclei. The complete coalescence of the crystals touching each other is a grain coarsening resulting also in the development of discrete single crystals and connected to some changes in the orientation controlled mainly by the minimisation of the substrate–crystal interface energy. The intersection lines of the crystal side faces and the substrate present a structure precondition specific for the growth of these crystals.

When a crystal becomes part of a polycrystalline structure, it might have various grain sizes and orientations as well as surface conditions. These structure conditions will determine its behaviour in the collective crystal growth characterising the polycrystalline film structure. The growing faces of a crystal are parts of the free surface of the film. These crystal faces correspond to the equilibrium crystal shape and are determined by the orientation of the crystal at high purity conditions. A growth competition can start among the neighbouring crystals in case of different orientation according to the types of their growing faces, i.e., to their orientation [61–63]. For example, the faster growing crystals will grow over the slower growing ones developing V-shaped crystal forms; this growth is illustrated in Figs. 2. This competition is terminated when only crystals exhibiting the same type of crystal faces proceed to the free surface.

This competitive crystal growth represents an orientation selection among the crystals resulting in the so called competitive growth texture [64]. The consequence of this competitive growth is the development of a changing morphology and texture as illustrated by Figs.1 and 4. This is very pronounced at substrate temperatures where grain boundary migration is negligible. In that case, a small grained structure (corresponding mainly to the nucleation density) of random orientation exists in the substrate-near part of the film. It is followed by a part of V-shaped grains accompanied by an increase of the volume of preferentially oriented crystals [65]. This process could be concluded later in the development of a columnar structure with a nearly unique crystal orientation. The intersection lines of grain boundaries with the free surface can be active (this is the high purity case). Or passive (this is the case of the contaminated grain boundaries) in the monolayer nucleation. Consequently, in the presence of impurities, the property of the grain boundaries will determine the surface area where the segregated surface covering layer will develop [51].

The above analysis indicates that the higher cooling rate promotes the growth of (100) oriented VO_2 grains. This preferred growth orientation of VO_2 films has an important bearing and quite often may modify the physical properties. The above observations are important in correlating the growth and structure with the morphological and physical properties of the films.

The thermochromic properties of the films were studied by measuring the optical transmittance spectra and hysteresis loops for the samples (see Figs. 5 and 6). As shown in Fig. 5, all of the films show a transmittance of about 30% in the visible and a switching in the NIR. It is clearer observed at a temperature above the transition temperature there is an enhancement on the transmittance in the visible while on the infrared region there is a drop in the transmittance. The influence of the cooling rate on the sharpness of the drop of the transmittance in the infrared is seen to be around 15% for the samples cooled at a rate of 5 and 25 ^{o}C/min while for the samples cooled between 10 and 20 ^{o}C/min the transmittance dropped in the infrared about 11%.

To evaluate the transition temperature as well as the hysteresis width as function of the substrate temperature cooling rate, the derivatives of the transmittance (Tr) dependence of temperature (dTr/dT) were extracted for the VO_2 films at different temperature. A plot of (dTr/dT) was obtained from the transmittance (Tr)–temperature (T) data at different temperature from 25 ^{o}C to 100 ^{o}C. The maximum temperature corresponding to (dTr/dT) was defined as the phase temperature in the heating and cooling cycle, $T_{heating}$ and $T_{cooling}$, respectively. The IMT temperature (T_{IMT}) was defined as $T_{IMT} = \left(T_{Heating} + T_{Cooling}\right)/2$. The hysteresis width can be defined by $\Delta T_{IMT} = T_{Heating} - T_{Cooling}$.

Fig. 7 reports on the transition temperature of the VO_2 thin films as function of cooling rate, while Fig. 8 reports on the hysteresis widths as function of the cooling rate. For films grown at higher temperature cooling rate, the transition temperature (T_{IMT}) increased, but a minimum hysteresis of 4.8 ^oC for the samples prepared at a cooling rate of 25^oC/min appeared. However, films grown at a cooling rate of 5^oC/min showed a large hysteresis of 26.5 ^oC with a much smaller transition at a cooling rate of 10^oC/min. The films of VO_2 on the glass substrates presumably have random nanocrystalline grains with high defect densities, and the properties are certainly correlated to their structural and microstructural properties. The difference in orientation, texturation and morphology as observed in the XRD and SEM results respectively for the different preparation conditions are making it likely that cooling rate has a great effect on the optical switching properties of the films. These differences in morphologies and orientations of the films lead to distinctive IMT characteristics seen in curves of Figs. 7 and 8. The changes of thermo-optical properties of VO_2 thin films are usually explained as results of the competing effects between grains size, nucleation defects, grains boundaries and crystal imperfections. Suh *et al.* [66] studied carefully IMT transition of VO_2 films on (100) silicon substrates as a function of annealing time where films microstructure changed from nanocrystalline nearly amorphous to 200 nm diameter. In early stages, the films showed as the grain size increased, the IMT decreased, but hysteresis continued to increase. Brassard *et al.* [16] studied the effect of grain size of random VO_2 polycrystalline films on amorphous Si_3N_4/Si (100) substrates. As the random grain size increased, the transition became sharper or ΔT decreased because of decreased defect content. However, hysteresis remained large because the boundaries stayed large angle, only their number density was reduced with increasing grain. As a result, we could conclude that the changes in the thermo-optical properties as reported in Figs 7 and 8 is a competition effect of the nucleating defects, dislocations, grain boundaries, grains sizes and crystal structure of the VO_2 films with the cooling rate.

4. Conclusion

The thin films of VO_2 were deposited onto the Soda lime glass by using the pulsed-laser deposition technique in which the control of post-deposition parameters promoted the quality of films structure. We have focused our attention on the influence of the cooling rate of substrate temperature under vacuum after deposition, on the structure, surface morphology and the optical switching properties. XRD data suggest that the VO_2 thin films exhibited a predominantly (100) orientation. It is observed that the crystallinity of the film increases with increasing the cooling rate. However, it was showed that a recrystallization process took place when the

temperature cooling rate is increased that lead to a preferential growth along the a-axis of the monoclinic when cooled to room temperature. A detailed description of the growth mechanisms and the substrate/film interaction is given, results on the surface morphology and grain boundary structure and the texturation are also presented. This study show that a-axis VO_2 textured can be gown on glass resulting from the nucleation of the substrate temperature of 600 ^oC followed by a recrystallization process.

The sharpness and the hysteresis width ΔT of T-dependent insulator-to-metal hysteretic phase transition in VO_2 were our most immediate and relevant quality indicators of the quality of the deposited a-axis oriented VO_2 on glass substrate.

5. Acknowledgments

We are thankful for financial support from UNESCO-UNISA Africa Chair in Nanosciences-Nanotechnology, INRS (Canada), the ICTP-Trieste and the NANOAFNET and also to iThemba LABS and the EMT-INRS for the use of their facilities.

6. References

[1] F. J. Morin, Phys. Rev. Lett. 3, 34 (1959).

[2] A. Cavalleri, C. Toth, C. W. Siders, J. A. Squier, F. Raksi, P. Forget, and J. C. Kieffer, Phys. Rev. Lett. 87, 237401 (2001).

[3] T. D. Manning, I. P. Parkin, R. J. H. Clark, D. Sheel, M. E. Pemble, and D. Vernadou, J. Mater. Chem. 12, 2936 (2002).

[4] S. Biermann, A. Poteryaev, A. I. Lichtenstein, and A. Georges, Phys. Rev. Lett. 94, 026404 (2005).

[5] Hyun-Tak Kim, Byung-Gyu Chae, Doo-Hyeb Youn, Sung-Lyul Maeng, Gyungock Kim, Kwang-Yong Kang and Yong-Sik Lim, New Journal of Physics **6** (2004) 52

[6] H. T. Kim, Y. W. Lee, B. J. Kim, B. G. Chae, S. J. Yun, K. Y. Kang, K. J. Han, K. J. Yee, and Y. S. Lim, Phys. Rev. Lett. 97, 266401 (2006).

[7] J. Narayan and V. M. Bhosle, J. Appl. Phys. 100, 103524 (2006).

[8] H. Zhou, M. F. Chisholm, Tsung-Han Yang, S. J. Pennycook, and J. Narayan J. Appl. Phys. 110, 073515 (2011)

[9] B. Lazarovits, K. Kim, K. Haule, and G. Kotliar, Phys. Rev. B 81, 115117 (2010).

[10] J. Nag and R. F. Haglund, J. Phys.: Condens. Matter 20, 264016 (2008).

[11] E. N. Fuls, D. H. Hensler, and A. R. Ross, Appl. Phys. Lett. 10, 199 (1967).

[12] G. A. Rozgonyi and D. H. Hensler, J. Vac. Sci. Technol. 5, 194 (1968).

[13] C. H. Griffths and H. K. Eastwood, J. Appl. Phys. 45, 2201 (1974).

[14] K. D. Rogers, J. A. Coath, and M. C. Lovell, J. Appl. Phys. 70, 1412 (1991).

[15] H. J. Schlag and W. Scherber, Thin Solid Films 366, 28 (2000).

[16] D. Brassard, S. Fourmaux, M. Jean-Jacques, J. C. Kieffer, and M. A. El Khakani, Appl. Phys. Lett. 87, 05191 (2005).

[17] E. E. Chain, J. Vac. Sci. Technol. A 4, 432 (1986).
[18] C. Chen, X. Yi, J. Zhang, and X. Zhao, Infrared Phys. Technol. 42,87 (2001).
[19] S. B. Wang, S. B. Zhou, G. Huang, and X. J. Yi, Surf. Coat. Technol. 191, 330 (2005).
[20] J. Li and N. Yuan, Proc. SPIE 5774,232 (2004).
[21] J. H. Li, N. Y. Yuan, and J. S. Xie, Appl. Surf. Sci. 243, 437 (2005).
[22] K. van Steensel, F. van de Burg, and C. Kooy, Philips Res. Rep. 22, 170 (1967).
[23] G. A. Nyberg and R. A. Buhrman, J. Vac. Sci. Technol. A 2, 301 (1984).
[24] S. Koide and H. Takei, J. Phys. Soc. Jpn. 22, 946 (1967).
[25] J. B. MacChesney, H. J. Guggenheim, and J. F. Potter, J. Electrochem. Soc. 115,52 (1968).
[26] H. K. Kim, H. You, R. P. Chiarello, H. L. M. Chang, T. J. Zhang, and D. J. Lam, Phys. Rev. B 47, 12900 (1993).
[27] V. N. Andreev, M. A. Gurvitch, V. K. Klimov, I. A. Khahaev, and F. A. Chudnovskiy, Tech. Phys. Lett. 19, 283 (1993).
[28] V. N. Andreev, F. A. Chudnovskiy, and V. K. Klimov, JETP Lett. 60, 647 (1994).
[29] D. H. Kim and H. S. Kwok, Appl. Phys. Lett. 65, 3188 (1994).
[30] Z. P. Wu, S. Yamamoto, A. Miyashita, Z. J. Zang, K. Narumi, and N. Naramoto, J. Phys.: Condens. Matter 10, L765 (1998).
[31] K. Nagashima, T. Yanagida, H. Tanaka, and T. Kawai, J. Appl. Phys. 100, 063714 (2006).
[32] F. A. Chudnovskiy and G. B. Stefanovich, J. Solid State Chem. **98**, 137 (1992);
[33] G. B. Stefanovich, A. L. Pergament, A. A. Velichko, and L. A. Stefanovich, J. Phys.: Condens. Matter **16**, 4013 (2004).
[34] D. P. Partlow, S. R. Gurkovich, K. C. Radford, and L. J. Denes, J. Appl. Phys. **70**, 444 (1991);
[35] Y. Ningyi, L. Jinhua, H. L. W. Chan, and L. Chenglu, Appl. Phys. A: Mater. Sci. Process. **78**, 777 (2004);
[36] M. Pan, H. Zhong, S. Wang, J. Liu, Z. Li, X. Chen, and W. Lu, J. Cryst. Growth **265**, 121 (2004).
[37] G. A. Rozgonyi and W. J. Polito, J. Electrochem. Soc. **115**, 56 (1968);
[38] P. J. Powell, C. N. Bergland, and W. E. Spicer, Phys. Rev. **178**, 1410 (1969).
[39] I. Balberg and S. Trokman, J. Appl. Phys. **46**, 2111 (1975).
[40] A. A. Bugaev, B. P. Zakharchenya, and F. A. Chudnovskiy, Sov. J. Quantum Electron. **9**, 855 (1979).
[41] S.-J. Jiang, C.-B. Ye, M. S. R. Khan, and C.-G. Granqvist, Appl. Opt. **30**, 847 (1991).
[42] G. Golan, A. Axelevitch, B. Sigalov, and B. Gorenstein, Microelectron. J. **34**, 255 (2003).
[43] V. I. Andreev, A. S. Oleinik, and Yu. I. Sarov, Sov. Phys. Solid State **22**, 2163 (1980);
[44] Y.-H. Han, I.-H. Choi, H.-K. Kang, J.-Y. Park, K.-T. Kim, H.-J. Shin, and S. Moon, Thin Solid Films **425**, 260 (2003).
[45] J. He, L. Lin, Y. Lu, T. Lu, Z. Liu, and J. Wang, Proc. SPIE **6037**, 429 (2006).
[46] G. Garry et al. / Thin Solid Films 453 –454 427–430 (2004).
[47] T.-W. Chiu et al. / Thin Solid Films 518, 7441–7444 (2010).
[48] S. Lu, L. Hou, Thin Solid Films 353 40-44 (1999).
[49] Wang Xue-Jin, Liang Chun-Jun, Guan Kang-Ping,Li De-Hua, Nie Yu-Xin, Zhu Shi-Oiu, Huang Feng, Zhang Wei-Wei, and Cheng Zheng-Wei, Chinese Physics B.173514 (2008).

[50] J. F. Pocza, A. Barna, P.B. Barna, I. Pozsgai, G. Radnoczi, Jpn. J. Appl. Phys. 2 1974 525, Part 1.

[51] P.B. Barna, G. Radnoczi, F.M. Reicha, Vacuum 38 527 (1988).

[52] M. Menyhard, L. Uray, Scr. Metall. 17 1983 (1195).

[53] L. Uray, M. Menyhard, Phys. Status Solidi A 84 65 (1984).

[54] P. B. Barna, M. Adamik, in: F.C. Matacotta, G. Ottaviani Eds., Science and Technology of Thin Films World Scientific Publ., Singapore, 1 (1995).

[55] G. Zinsmeister, Thin Solid Films 2 497 (1968).

[56] B. Lewis, J. C. Anderson, Nucleation and Growth of Thin Films, Academic Press, London, (1978).

[57] L. Eckertova, Physics of Thin Films, Plenum, New York, (1977)

[58] R. Anton, M. Harsdorff, Th. Martens, Thin Solid Films 57 233 (1979).

[59] A.D. Gates, J.C. Robins, Thin Solid Films 149 113 (1987).

[60] J.A. Venables, G.D.T. Spiller, M. Hanbrucken, Rep. Prog. Phys. 47 399 (1984).

[61] J.E. Greene, in: R.F. Bunshah Ed. , Handbook of Deposition Technologies for Films and Coatings, Chap. 13, Noyes Publications, Park Ridge, 681 (1994).

[62] A. van der Drift, Philips Res. Rep. 22 267 (1967).

[63] G. Knuyt, C. Quaeyhaegens, J. D'Haen, L.M. Stals, Thin Solid Films 258 159 (1995).

[64] G. Knuyt, C. Quaeyhaegens, J. D'Haen, L.M. Stals, Phys. Status Solidi B 195 179 (1996).

[65] M. Adamik et al., Thin Solid Films 317 64–68 (1998)

[66] J. Y. Suh, R. Lopez, L. C. Feldman, and R. F. Hagland, J. Appl. Phys. 96, 1209 (2004).

Figure Caption

Fig.1: XRD pattern characteristic of VO_2 thin films deposited on soda lime glass substrate and cooled down to room temperature with different cooling rate under vacuum.

Fig.2: Evolution as function of the cooling rate of the intensity ration of the (011) plane to the (100) Plane.

Fig.3: Evolution as function of the cooling rate of: (A) The $d_{(100)}$-spacing; (B) The $d_{(011)}$-spcaing (C) the Crystallites size along the (100) plane; (D) the Crystallites grains size along the (011) plane.

Fig.4: 2D SEM images of the VO_2 samples as function of substrate cooling rate.

Fig.5: Optical transmittance (%) vs. wavelength at two different temperatures of VO_2 thin films deposited on soda lime glass substrate and cooled down to room temperature with different cooling rate under vacuum,

Fig.6: Optical transmittance (%)'s hysteresis loops vs. wavelength of VO_2 thin films deposited on soda lime glass substrate and cooled down to room temperature with different cooling rate under vacuum.

Fig.7: Evolution as function of the cooling rate of: the transition temperature characteristic of VO_2 thin films deposited on soda lime glass substrate and cooled down to room temperature with different cooling rate under vacuum.

Fig.8: Evolution as function of the cooling rate of the hysteresis characteristic of VO_2 thin films deposited on soda lime glass substrate and cooled down to room temperature with different cooling rate under vacuum.

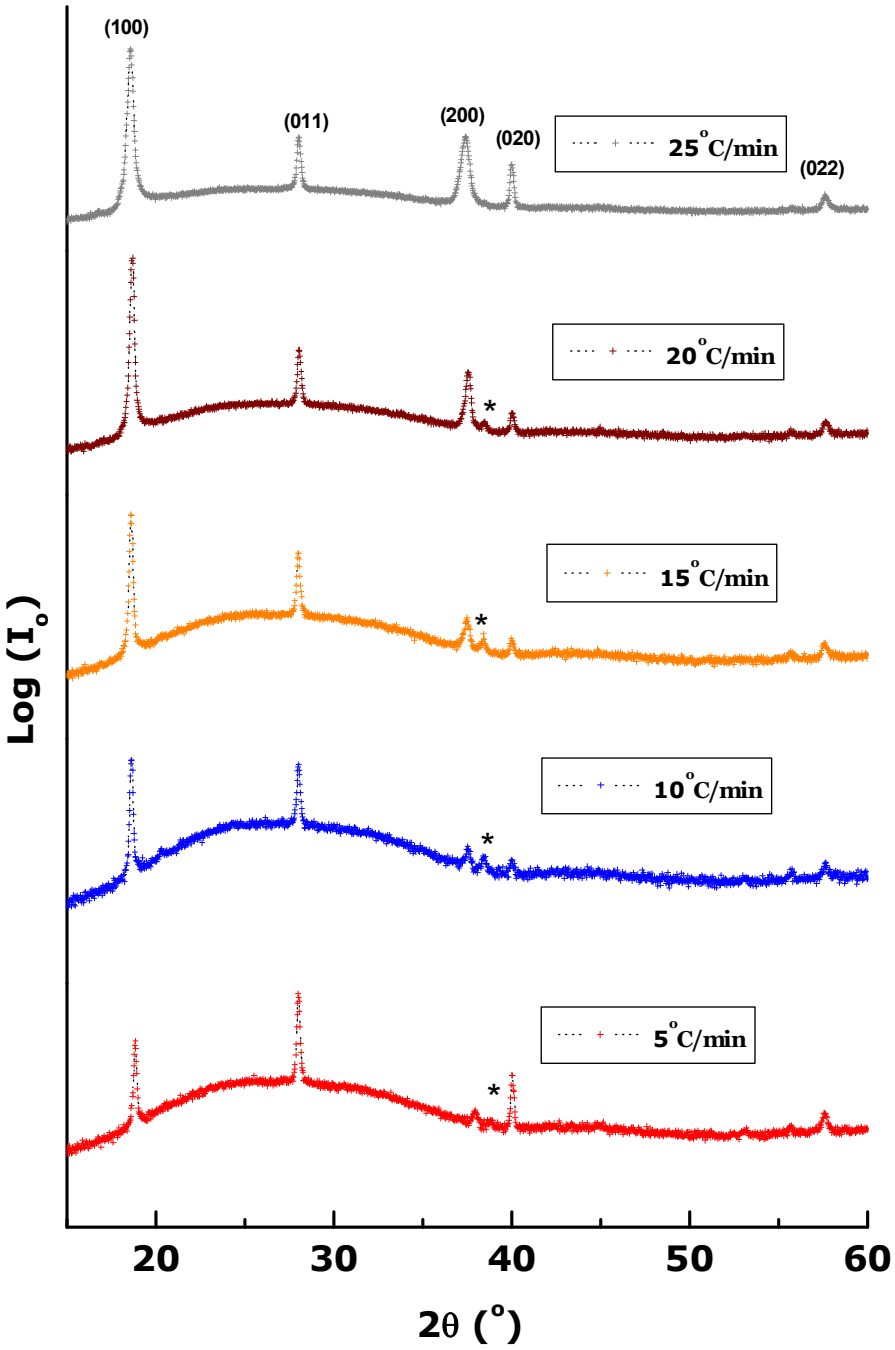
(100)
(011)
(200)
(020)
(022)
25°C/min
20°C/min
15°C/min
10°C/min
5°C/min
*
Log (I°)
20
30
40
50
60
2θ (°)

Fig.1

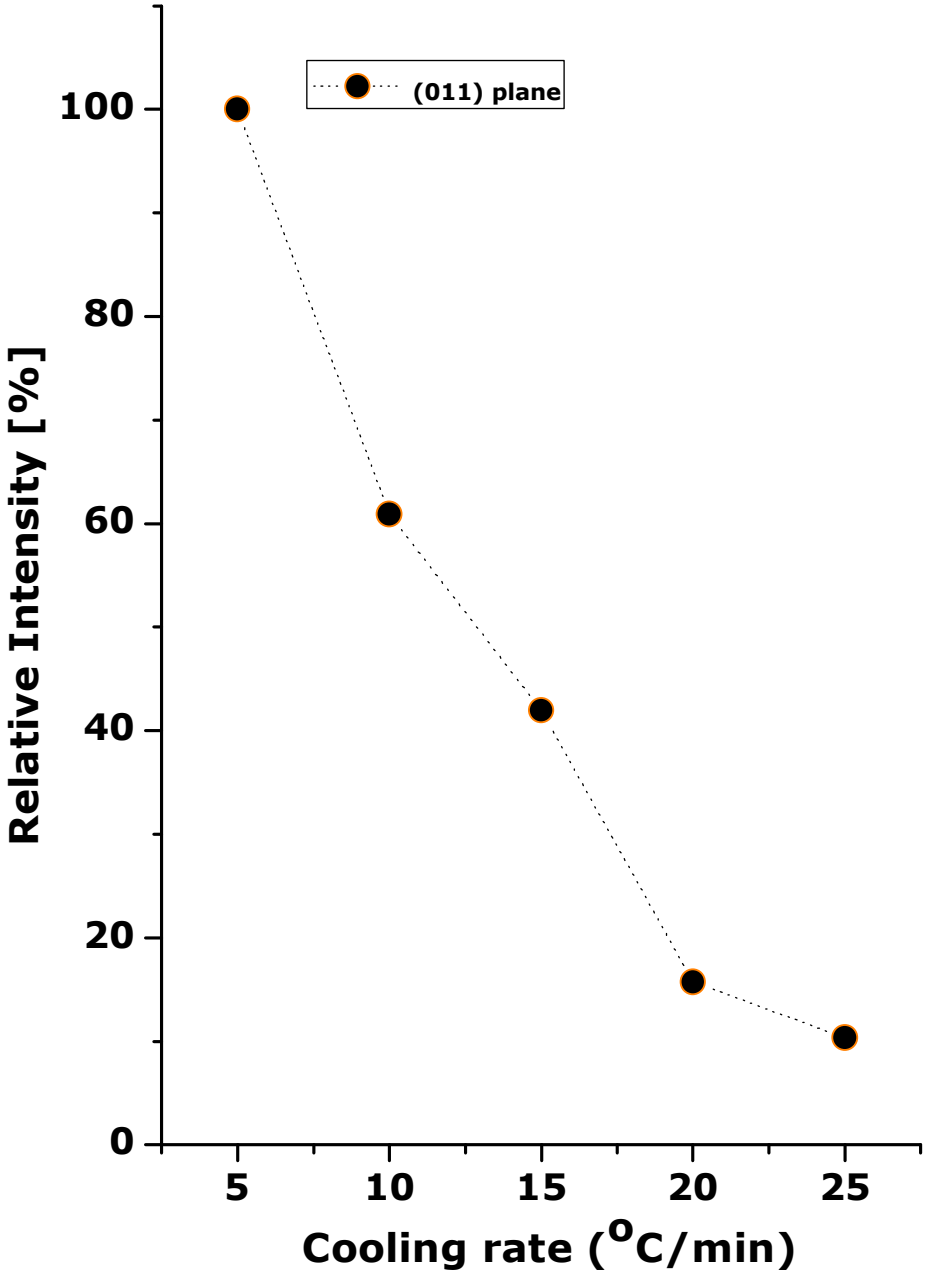
(011) plane
Relative Intensity [%]
100
80
60
40
20
0
5
10
15
20
25
Cooling rate (°C/min)

Fig.2:

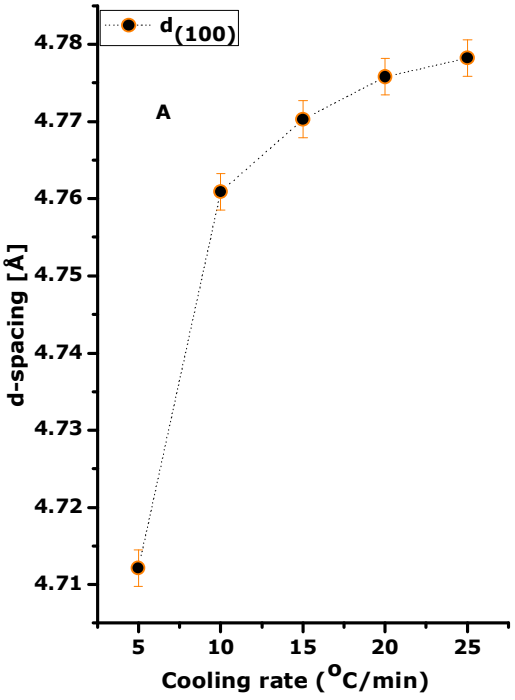
d(100)
A
d-spacing [Å]
Cooling rate (°C/min)

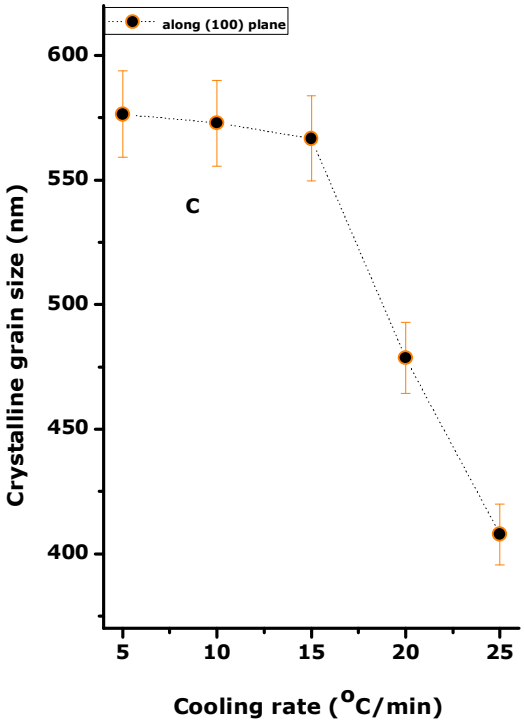
along (100) plane
C
Crystalline grain size (nm)
Cooling rate (°C/min)

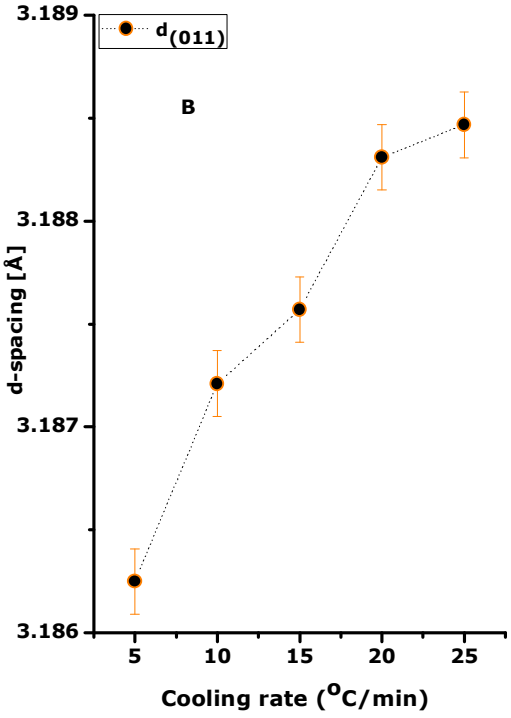
d(011)
B
d-spacing [Å]
Cooling rate (°C/min)

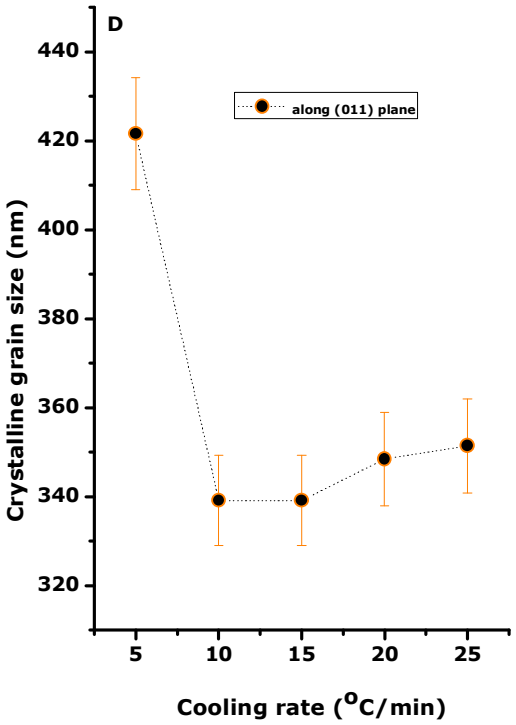
D
along (011) plane
Crystalline grain size (nm)
Cooling rate (°C/min)

Fig.3:

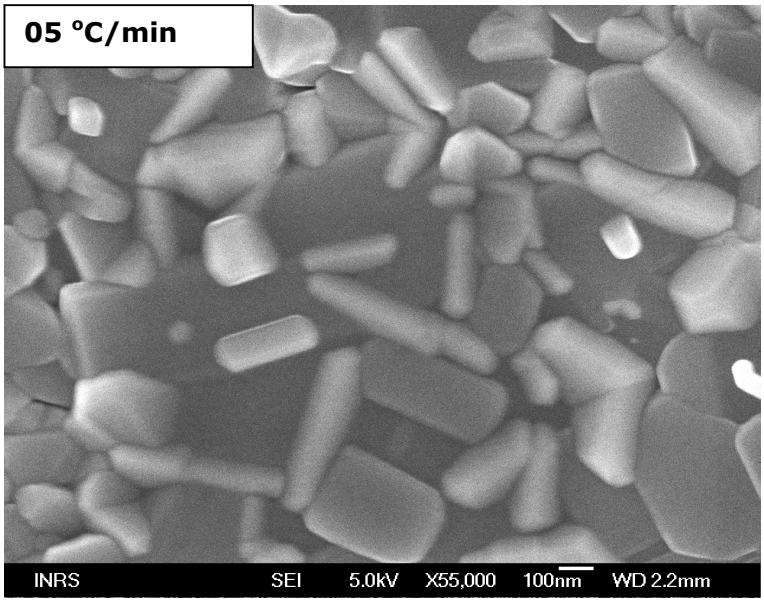
05 °C/min
INRS SEI 5.0kV X55,000 100nm WD 2.2mm

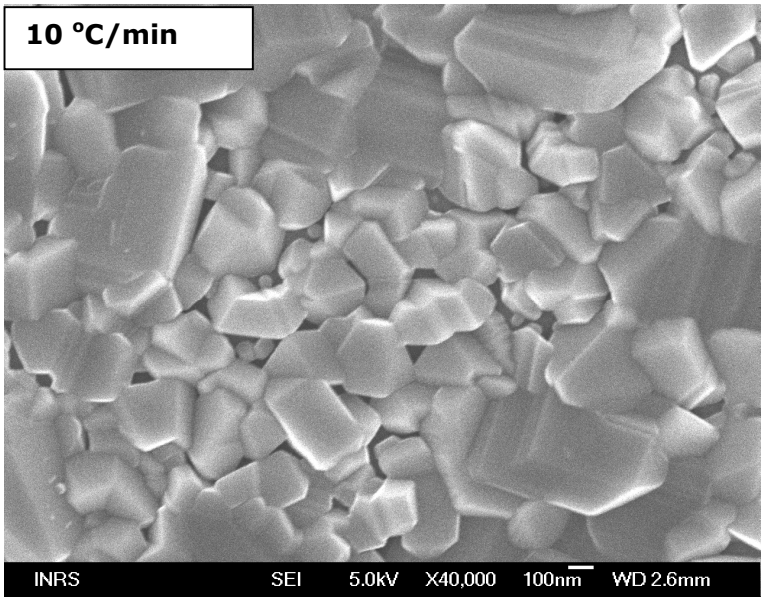
10 °C/min
INRS SEI 5.0kV X40,000 100nm WD 2.6mm

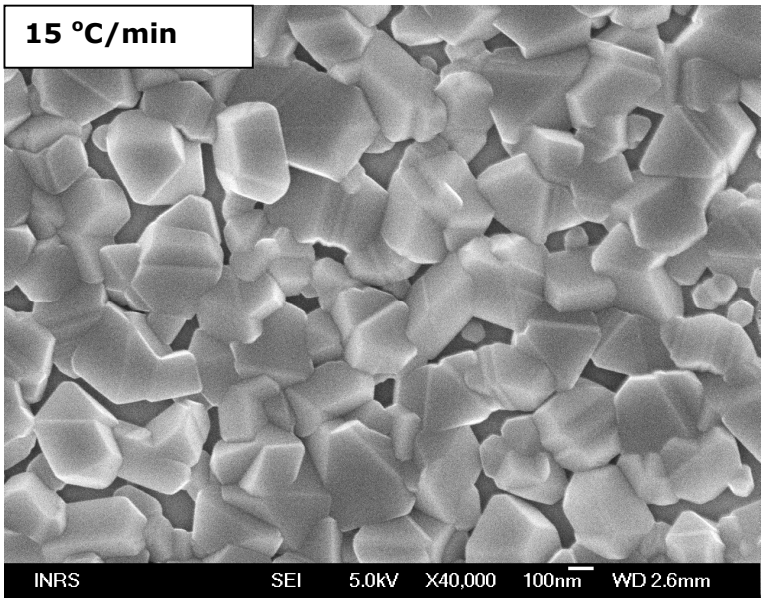
15 °C/min
INRS SEI 5.0kV X40,000 100nm WD 2.6mm

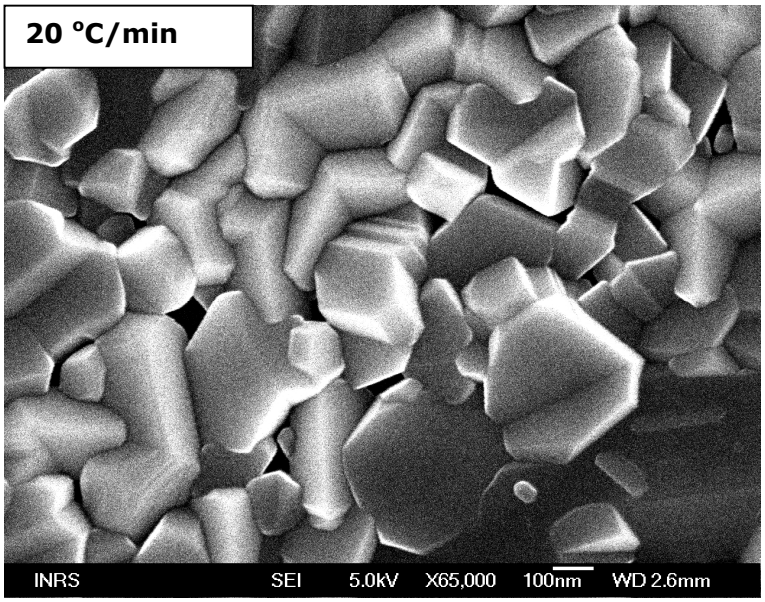
20 °C/min
INRS SEI 5.0kV X65,000 100nm WD 2.6mm

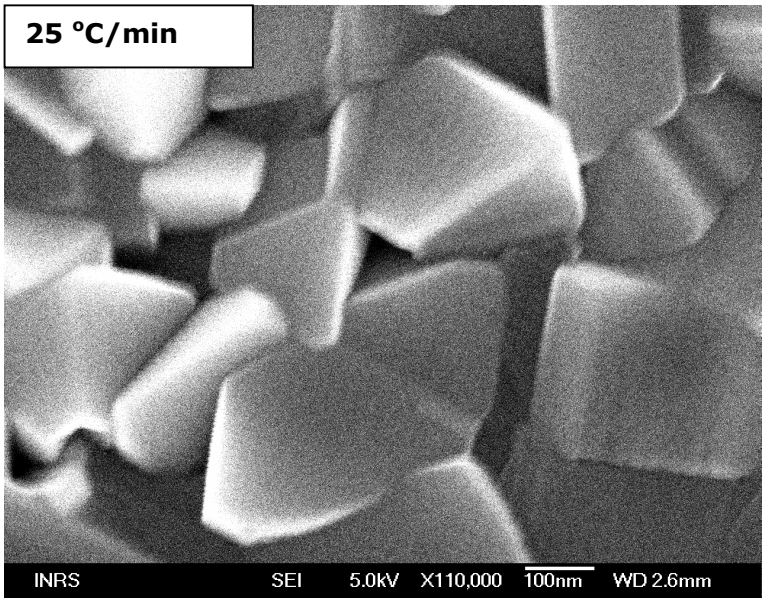
25 °C/min
INRS SEI 5.0kV X110,000 100nm WD 2.6mm

Fig.4:

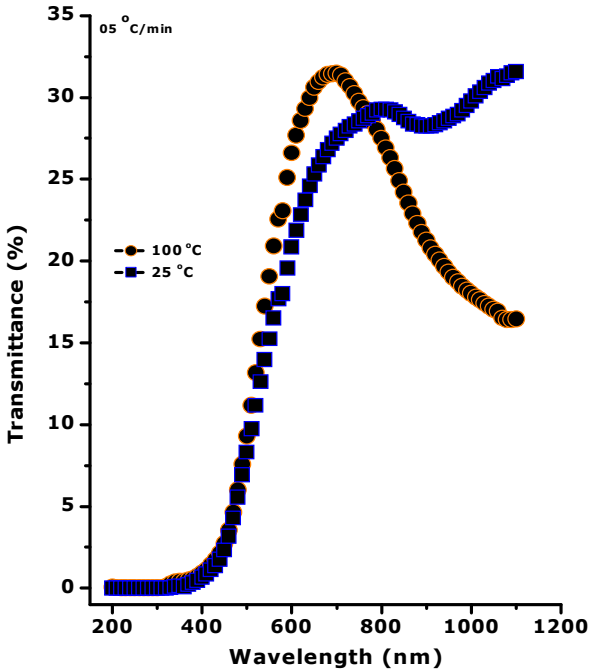
05 °C/min
100 °C
25 °C
Transmittance (%)
Wavelength (nm)

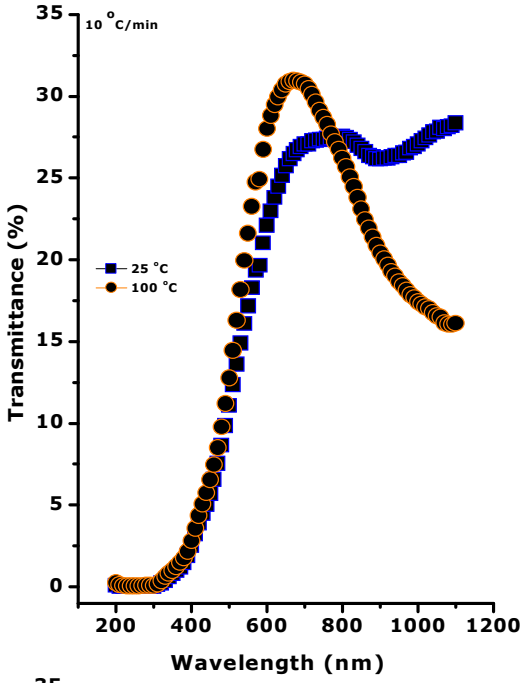
10 °C/min
25 °C
100 °C
Transmittance (%)
Wavelength (nm)

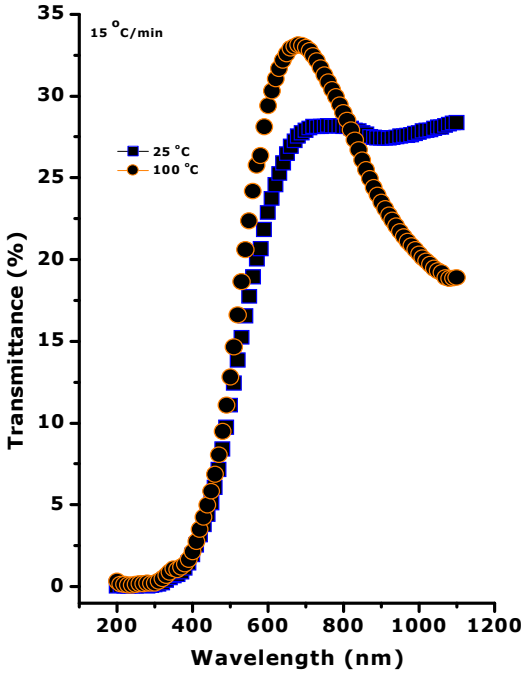
15 °C/min
25 °C
100 °C
Transmittance (%)
Wavelength (nm)

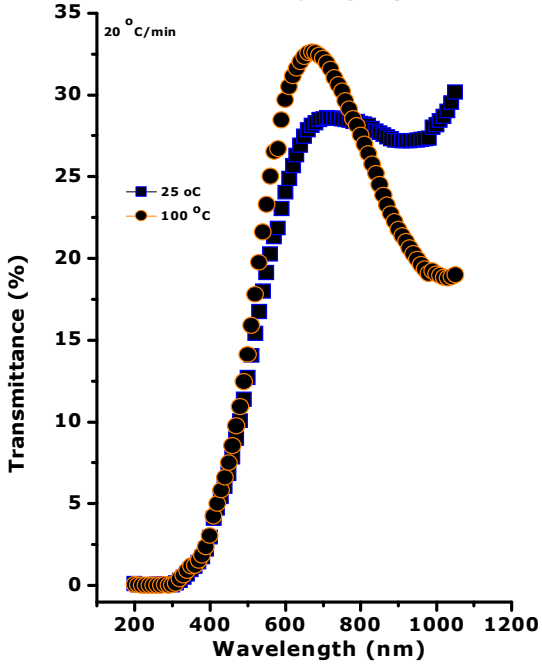
20 °C/min
25 oC
100 °C
Transmittance (%)
Wavelength (nm)

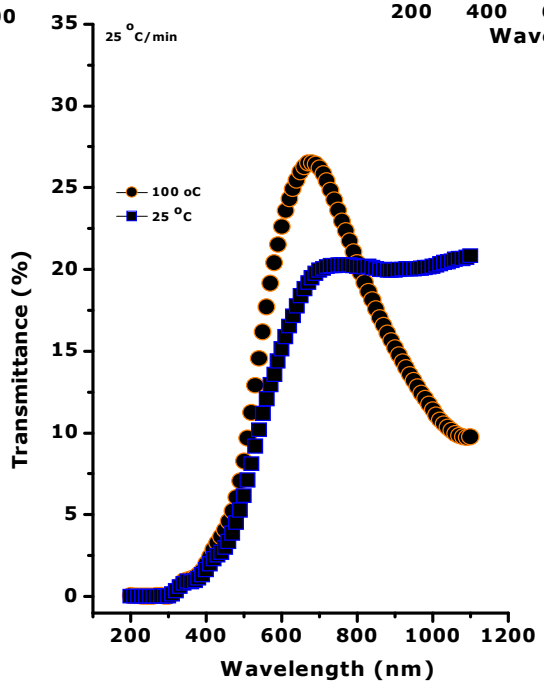
25 °C/min
100 oC
25 °C
Transmittance (%)
Wavelength (nm)

Fig.5:

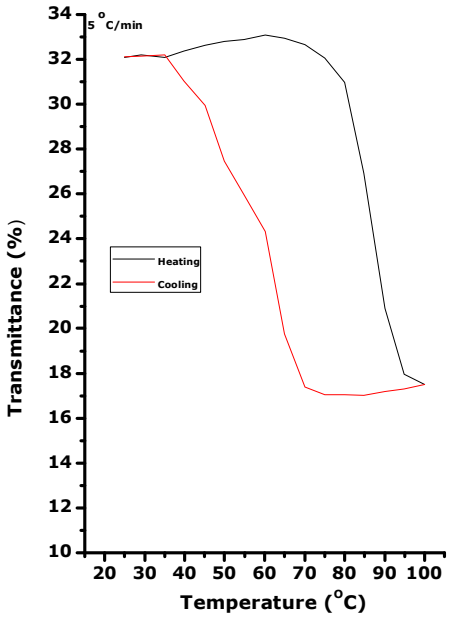
5 °C/min
Heating
Cooling
Transmittance (%)
Temperature (°C)

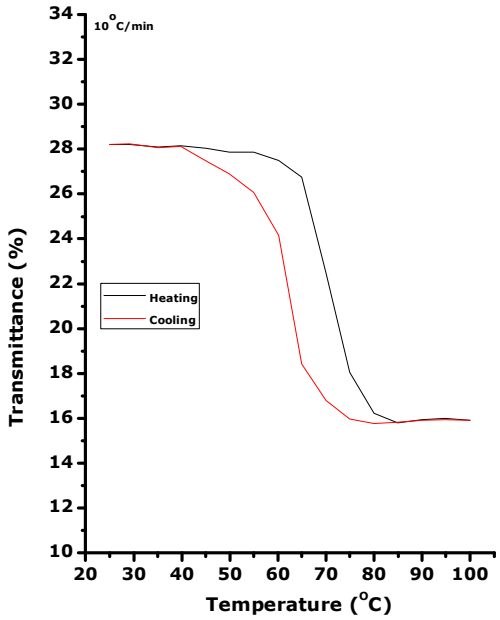
10 °C/min
Heating
Cooling
Transmittance (%)
Temperature (°C)

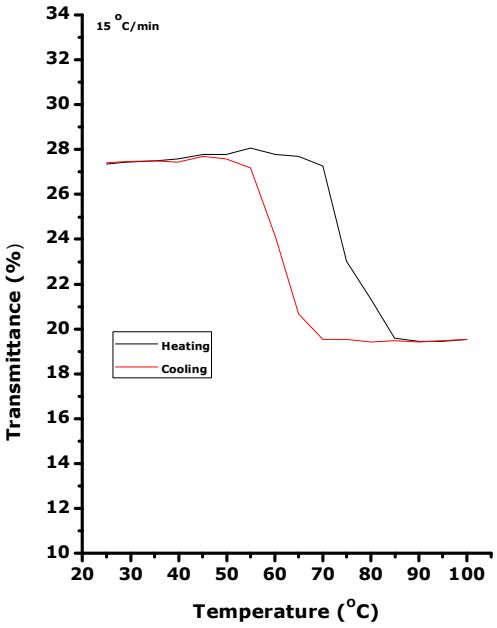
15 °C/min
Heating
Cooling
Transmittance (%)
Temperature (°C)

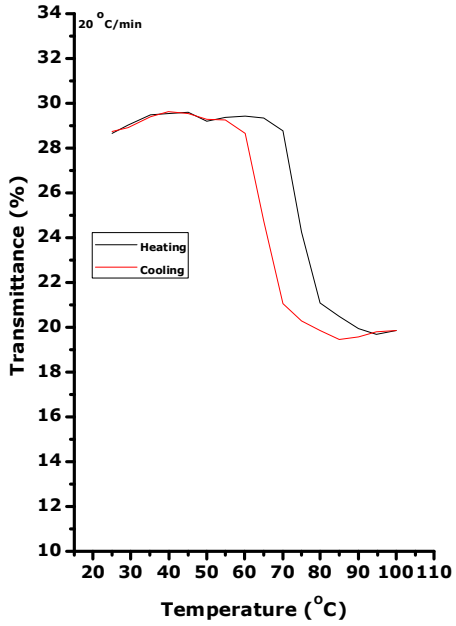
20 °C/min
Heating
Cooling
Transmittance (%)
Temperature (°C)

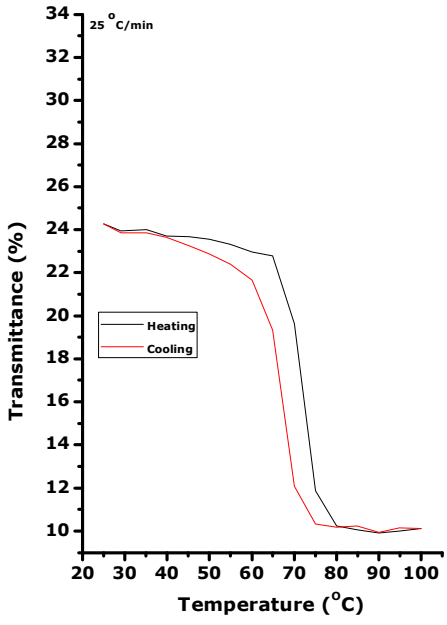
25 °C/min
Heating
Cooling
Transmittance (%)
Temperature (°C)

Fig.6

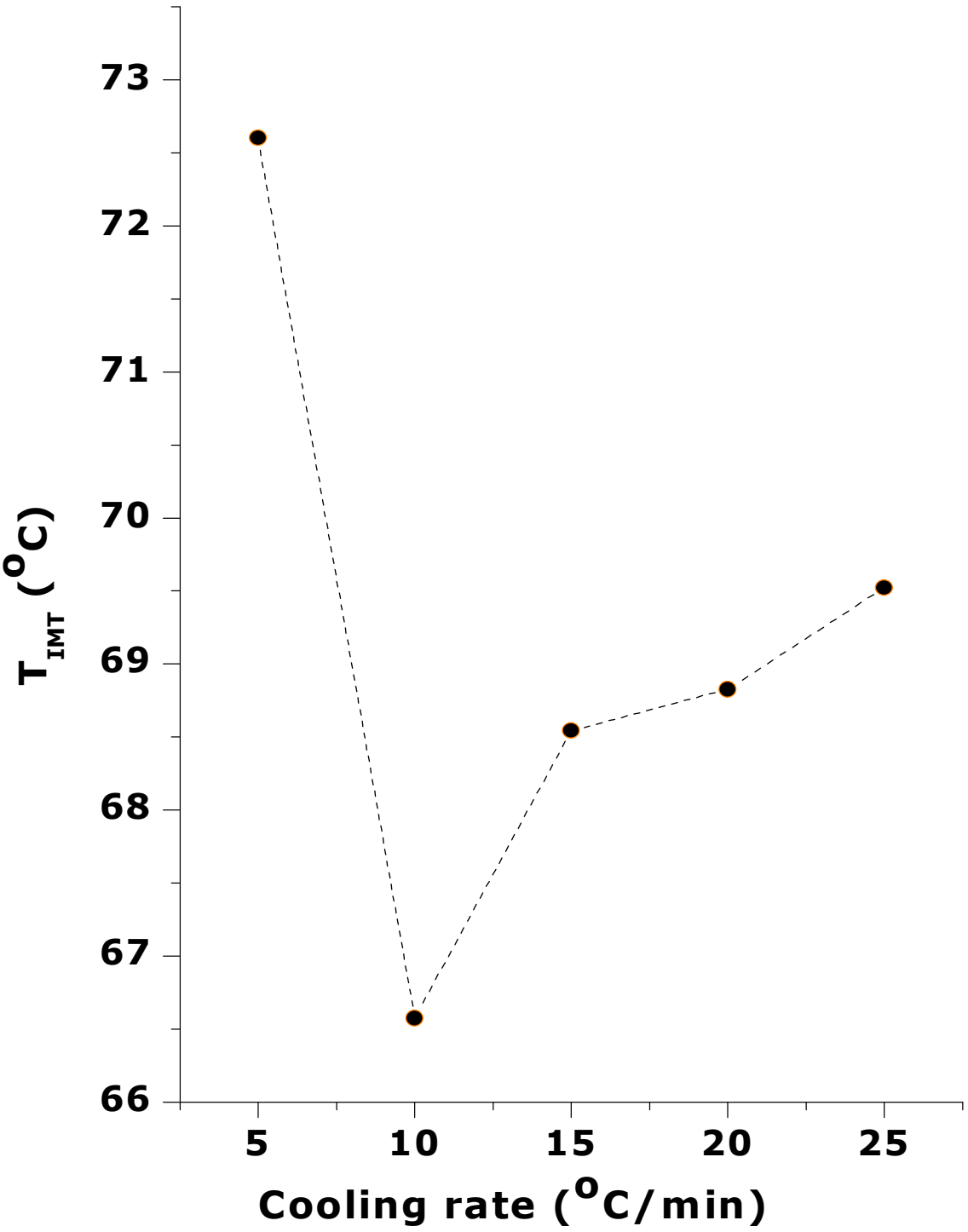

Fig.7

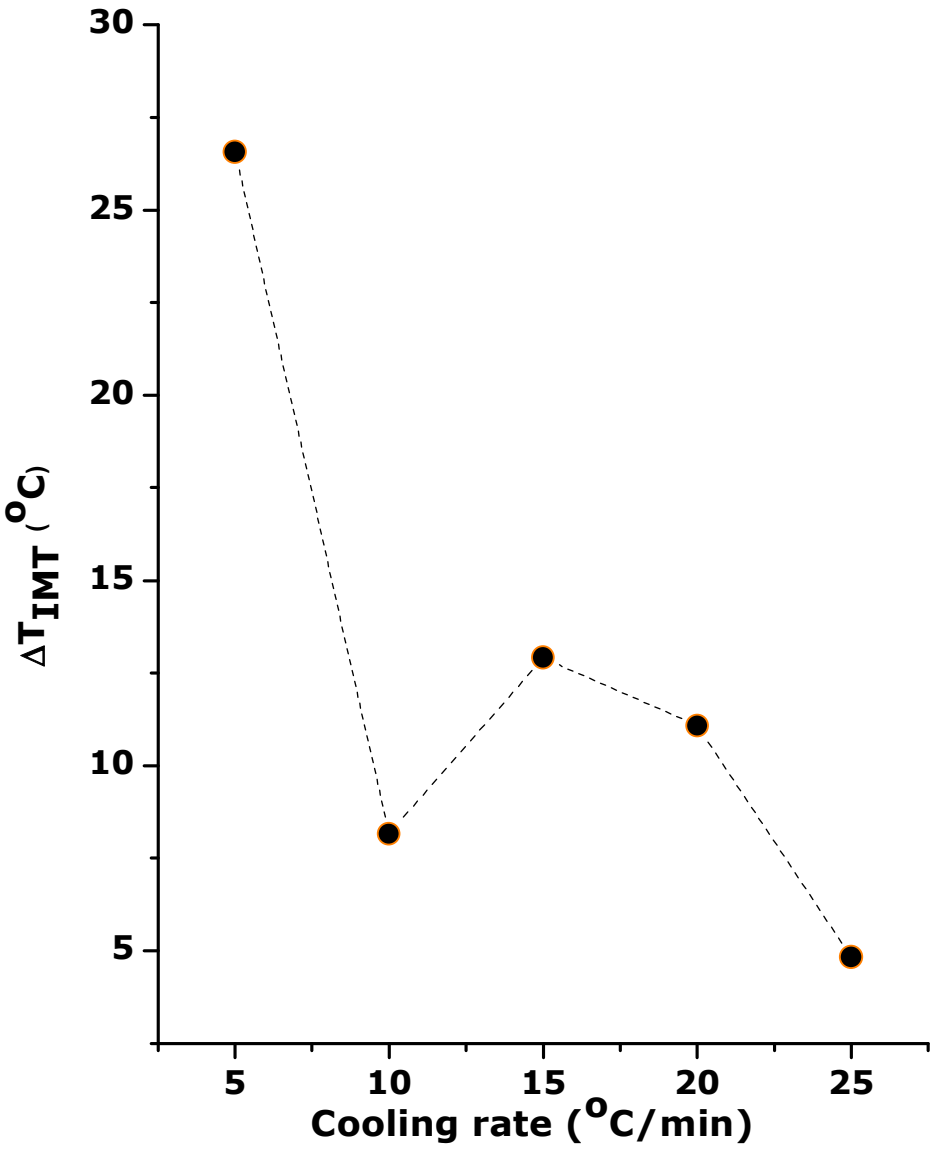

Fig.8